Kähkönen, Henri; Ala-Laurinaho, Juha; Viikari, Ville

Dual-Polarized Ka-Band Vivaldi Antenna Array

Published in:
IEEE Transactions on Antennas and Propagation

DOI:
10.1109/TAP.2019.2948561

Published: 01/04/2020

Document Version
Publisher's PDF, also known as Version of record

Dual-Polarized Ka-Band Vivaldi Antenna Array

Henri Kähkönen, Juha Ala-Laurinaho, and Ville Viikari, *Senior Member, IEEE*

***Abstract*— This article presents a high-performance fully metallic dual-polarized wideband Vivaldi array for the *Ka*-band (26–40 GHz), which is going to be used, for example, in 5G millimeter-wave (mmWave) communication networks. Antenna-array elements are fed straight from a single printed circuit board (PCB) that allows integrating active components in the immediate proximity of antenna elements. A whole array can be placed on a PCB as a through-hole or surface-mount technology component. The antenna is simulated in a unit cell with periodic boundary conditions and in an 8 × 8 array configuration. The simulations show that the active reflection coefficient is below −10 dB across the entire *Ka*-band and throughout most of the beam-steering angles up to ±60°. Lower than 3 dB scan loss is achieved in approximately ±60° range in the elementary planes and ±50° in the diagonal planes. The reflection coefficient and gain of each of the four elements in different parts of the manufactured dual-polarized 8 × 8 array were measured and simulated with the remaining elements terminated with a 50 Ω load. The measured results follow closely the full-wave finite array simulation results; the reflection coefficient is low and the element pattern is wide over the entire frequency range.**

***Index Terms*— 5G, antenna array, electronically scanned array, flared-notch antenna, *ka*-band, phased array, tapered slot, Vivaldi antenna, wideband.**

I. Introduction

PHASED arrays have long been used in radar, sensor, and communication applications where electrical beam steering or beamforming is more beneficial compared to fixed aperture and mechanical steering. The most pronounced benefits of phased arrays are virtually instant beam steering, a more robust structure without moving parts, smaller physical volume, and the possibility to manipulate the shape of the radiation pattern flexibly. Beam-steerable antennas are foreseen to be particularly useful in many applications at centimeter- and millimeter-wave (mmWave) frequencies, such as 5G, imaging systems, industrial sensors, and military applications [1]–[3]. Convergence of these applications is also foreseen. As an example, 5G base stations could operate as a multi-static radar for environmental sensing [4]. The *Ka*-band (26–40 GHz) is of particular interest, which, for example, covers many foreseen 5G mmWave frequencies.

Manuscript received March 18, 2019; revised September 10, 2019; accepted October 12, 2019. Date of publication November 7, 2019; date of current version April 7, 2020. This work was supported by Saab AB. *(Corresponding author: Henri Kähkönen.)*

H. Kähkönen is with the Department of Electronics and Nanoengineering, Aalto University, 02150 Espoo, Finland, and also with Saab Finland Oy, 00100 Helsinki, Finland (e-mail: henri.kahkonen@aalto.fi).

J. Ala-Laurinaho and V. Viikari are with the Department of Electronics and Nanoengineering, Aalto University, 02150 Espoo, Finland.

Color versions of one or more of the figures in this article are available online at http://ieeexplore.ieee.org.

Digital Object Identifier 10.1109/TAP.2019.2948561

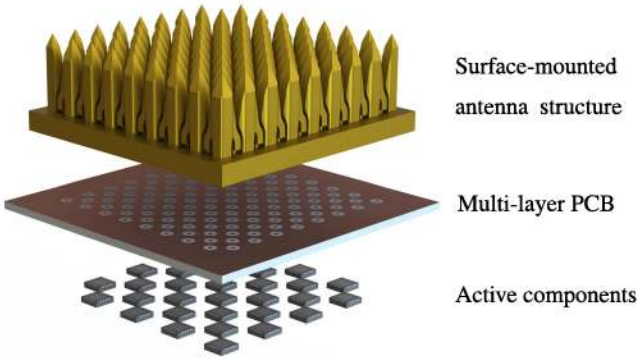

Fig. 1. Exploded view of the proposed integrated structure comprising three distinctive layers: the antenna structure, the multilayer PCB including the RF- and control signal paths, and the integrated electronics feeding the antennas.

In these new applications, a small and low-profile form factor is advantageous. For example, the increasingly dense base-station networks for telecommunications benefit from small and imperceptible base stations that are more easily deployed on indoor and outdoor walls. The advances in integrated circuits (ICs) allow cheaper and more complex electronics even for large phased arrays. Regardless of whether the phased array is fully digital or based on RF phase shifters, at mmWave frequencies, IC chips need to be integrated in the close proximity of the antenna element to minimize losses in the feed network. This, in combination with an antenna design allowing the ICs to be implemented close to the antennas, enables compact packaging for both the antenna and the transceiver, for example, integrating the antenna and the electronics with a single-interface printed circuit board (PCB), as shown in Fig. 1. On the downside, integrating a large amount of high-power electronics in a small area creates heat which has to be dissipated. The fully metallic antenna structure presented here could ideally be used as a heat sink to increase heat dissipation.

Some research has been done on phased arrays for the *Ka*-band, but the published structures do not cover the entire frequency band, have a wide enough scan range, or are rather bulky [5]–[8]. The previously studied structures are usually variations of microstrip patch antennas, on-chip antennas, reflectarrays, or lens antennas. Microstrip patch antennas are easy to manufacture but usually have a narrow bandwidth and might suffer from surface waves. On-chip antennas usually suffer from high losses, and they are hard to manufacture in large continuous arrays. Reflectarrays and lens antennas, on the other hand, are large, usually suffer from low efficiency, and do not provide a large beam-steering range.

Vivaldi antennas are known to behave well in arrays, and they have been extensively studied. While Vivaldi antenna arrays up to 75 GHz have been shown [9], published research presenting performance results and a detailed description of the feeding structures, however, only covers frequencies up to 21 GHz [9]–[16]. Usually, the Vivaldi arrays have been manufactured using meshed PCBs of end-fire antennas, but fully metallic structures have also been studied. Furthermore, the Vivaldi antennas do not suffer from surface waves like many microstrip antennas do. They can also have a very wide bandwidth, even up to 12:1 [12], making them ideal for wideband phased arrays. The very wide bandwidth of the Vivaldi array enables a single-antenna design to be used in multiple narrowband applications within the operating region of the antenna, which decreases the need to design multiple antennas for different frequencies. For example, a single Vivaldi antenna array covering the Ka-band could be used in 5G mmWave telecommunication networks, which are planned to be operated in the 28 and 38 GHz bands [2].

A Vivaldi array can be manufactured as a single-metal part, simplifying the assembly of the antenna array. A particularly interesting element design proposed in [9] and [12] has a very wide bandwidth and works well within the specified $\pm 45°$ scan range, but the length of the antenna element causes it to suffer from very high polarization degradation at the higher end of the specified frequency range beyond 40° scan in diagonal planes. Two different solutions have been proposed to correct the polarization characteristics of Vivaldi antenna arrays in the diagonal plane. The first solution adds another layer of material to replace the top half of the cones in the antenna elements [15]. The downside of this solution is the more complex structure that might render this unfeasible for frequencies beyond 20 GHz due to the very small element size. The other solution used in [16] is to decrease the height of the antenna elements. This solution does not increase the complexity of the structure but has in general a negative impact on the bandwidth of the antenna.

A key question for developing antenna arrays at mmWave frequencies are the feeding of the antenna elements, the interface between the electronics and the antenna, and the measurements. Conventionally, Vivaldi arrays are fed through a separate connector for each antenna element which has allowed for a simple interface. At mmWave frequencies the element spacing is such that it is difficult and expensive to populate all the feeds with small connectors. Furthermore, the small size of the antenna element limits the realization of the antenna, especially the feed structure, increasing the importance of the single-piece design and low complexity of the array. Finally, the lack of connectors directly at each element complicates the measurement and characterization of the antenna array.

This article presents an antenna element based on an earlier study [17] of a beam-steerable antenna array in the Ka-band with a scan range of $\pm 60°$ in the elementary planes and $\pm 50°$ on the diagonal planes defined by the 3 dB scan loss. The presented antenna array covers the entire Ka-band with a simple single-element structure and an integrated coaxial feed. To the authors' knowledge, the presented antenna structure is the first published Vivaldi element design with measurement data covering the whole Ka-band and having a beam-steering capability of up to $\pm 60°$, with no large variation in the co-pol pattern. Additionally, due to the small size of the radiating elements and the integrated coaxial feed, the antenna array can be integrated directly on a PCB without connectors as a surfacemount or through-hole component, allowing the active electronics and the antenna to be integrated in a small package. Furthermore, the metal structure of the antenna can be used as a heat sink to cool the ICs if implemented on the PCB directly behind the antenna array.

This article is organized as follows: the antenna element structure and its simulated performance are presented in Section II; the manufacturing methods, the manufactured antenna structure, and the measurement setup are presented in Section III; followed by the measurement results, a comparison to simulation results, and a discussion about the results in Section IV; and Section V concludes this article.

II. Antenna Structure and Simulations

A. Antenna Element Structure

The objective of this research was to design a compact, dual-polarized antenna element for phased-array applications in the Ka-band, such that the antenna could be integrated on a PCB as a through-hole or surface-mount component without additional connectors. The antenna structure for Ka-band was first studied in [17], where the fundamental shape and operation of the structure were studied and simulated. The Vivaldi antenna (also known as a flared notch or tapered slot antenna) is widely known to have a large bandwidth both as a single isolated antenna and in an array configuration when correctly optimized [18]. In phased arrays, where the Vivaldi elements are placed close to each other, the mutual coupling between the elements is used to modify the impedance environment and to achieve concurrently the matching of the element.

In the Ka-band, the structure size is such that the design is mostly driven by the need to find the optimum between performance, structural strength, machining tolerances, and the complexity of the structure. The size of an antenna-array element is limited by the element spacing between each element, which generally is $\lambda/2$ to avoid any grating lobes when the beam is steered. Due to the small size of the structure, the proposed antenna array is constructed from a single metal part with an integrated coaxial feed. The advantage of the single-piece metal construction are simple assembly of the manufactured parts and rigid structure. The disadvantages of the one-piece metal structure is challenging and costly machining, limitations in the possible geometries that can be tooled, and that any major defect in only a small number of elements would necessitate the manufacturing of a new complete array.

The dual-polarized unit-cell model of the proposed structure for the Ka-band applications and the cross section of the radiating elements are shown in Fig. 2. The size of the cavity, the meandered slotline, and the length and the opening rate of the tapering slot were optimized in CST Studio Suite. The most critical optimized dimensions are shown in Table I. The antenna element is designed, so that an array of such

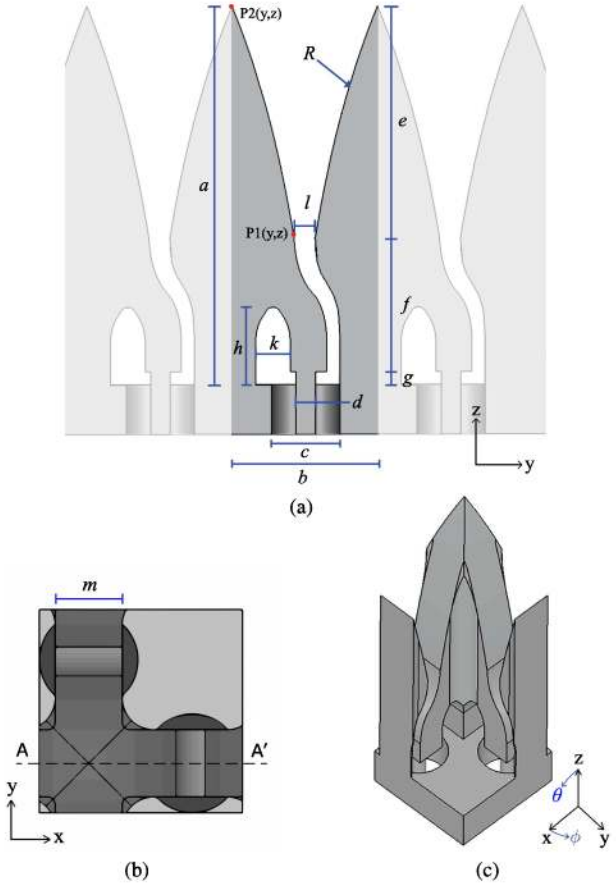

Fig. 2. Model of the simulated structure. (a) Cross section of the antenna element in an array cut along A–A', (b) top view, and (c) isometric view of the dual-polarized unit-cell model.

TABLE I
OPTIMIZED MODEL DIMENSIONS

Parameter	*a*	*b*	*c*	*d*
Value	9.9 mm	3.8 mm	1.8 mm	0.5 mm
Parameter	*e*	*f*	*g*	*h*
Value	6.05 mm	3.5 mm	0.35 mm	2 mm
Parameter	*m*	*R*	*k*	*l*
Value	1.25 mm	0.15	0.8 mm	0.55 mm

elements could be attached to and fed with a single-planar PCB behind the antenna array. Additionally, the limitations in manufacturing are taken into account, and some trade-offs between the performance and the manufacturability are necessary, e.g., with respect to the feeding of the antenna. The antenna feed structure consists of a vertical pin that is brought through the antenna ground plane as a coaxial line and couples to the meandered slot line at the base of the element. The meandered slot line has a small tapering before the exponential opening for improved matching. The curve for the exponentially opening slot is achieved as follows:

$$y = c_1 e^{Rz} + c_2 \tag{1}$$

where

$$c_1 = \frac{y_2 - y_1}{e^{Rz_2} - e^{Rz_1}} \tag{2}$$

$$c_2 = \frac{y_1 e^{Rz_2} - y_2 e^{Rz_1}}{e^{Rz_2} - e^{Rz_1}} \tag{3}$$

and R is the opening rate of the tapered slot. y_1 and z_1 are the coordinates of the starting point of the taper at the end of the meandered line section and y_2 and z_2 are the endpoints of the taper.

One crucial dimension is the thickness of the coaxial feeding pin to ensure its mechanical rigidity. Furthermore, the impedance of the coaxial pin should also be correct to match the slot line, defining the ratio between the inner and outer diameters of the coaxial feed. Taking these requirements into account, the total diameter of the feed is considerable when compared to the width of a single radiating element. Thus, a meandered slot line and a vertical feeding pin, as in [12], is used to keep the feeding structure as simple and structurally rigid as possible. This kind of feed structure can be fit completely under the radiating part, which increases the available space for realizing it. Using the vertical feed and the meandered slot line also enables the whole structure to be manufactured from a single block of metal, simplifying the assembly.

B. Antenna Simulations

A unit cell with a periodic boundary condition is used to simulate and design the antenna element with the assumption of an infinite array suitable for approximating large arrays. Such a simulation can be used to calculate the active reflection coefficient and the active element pattern of the antenna element in an infinite array [19]–[21]. If the objective is to design a relatively large array, e.g., 8 × 8 or larger, where the elements on the edges will have only a small effect to the total performance, such a simulation provides a good approximation of the performance of the antenna array. The unit-cell simulation results are presented in the E-, D-, and H-planes, which correspond to planes $\phi = 0°$, $\phi = 45°$, $\phi = 90°$, and $\phi = 135°$. The coordinate system with respect to the antenna is shown in Fig. 2(c).

Fig. 3 shows the simulated active reflection coefficients of the optimized antenna element in the three elementary planes as a function of frequency and the steering angle θ. The performance in all the presented planes are quite similar, which indicates that the reflection coefficient of the element is more dependent on the steering angle θ than on angle ϕ. With the exception of the small-edge cases close to $\theta = \pm 60°$ at $\phi = 90°$, the reflection coefficient is better than -10 dB in the whole steering and frequency range. The areas marked with black are the regions where the reflection coefficient is greater than -10 dB, the maximum being at -9 dB. There is a minimum in the reflection coefficient between steering angles $-40°$ and $40°$ approximately at 36 GHz. The minimum in the reflection coefficient is shifted to below 30 GHz when the array is steered more than 40°. Overall, the optimized structure provides a small reflection coefficient based on to the unit-cell simulation over the entire specified steering and frequency range.

The simulated coupling between the two polarizations is approx. -15 dB in the broadside direction and below -14 dB for the whole steering range. Fig. 4 shows the simulated coupling between the two orthogonal polarizations in an infinite array at $\theta = 0°$ and $\theta = 60°$ in the E-, D-, and H-planes.

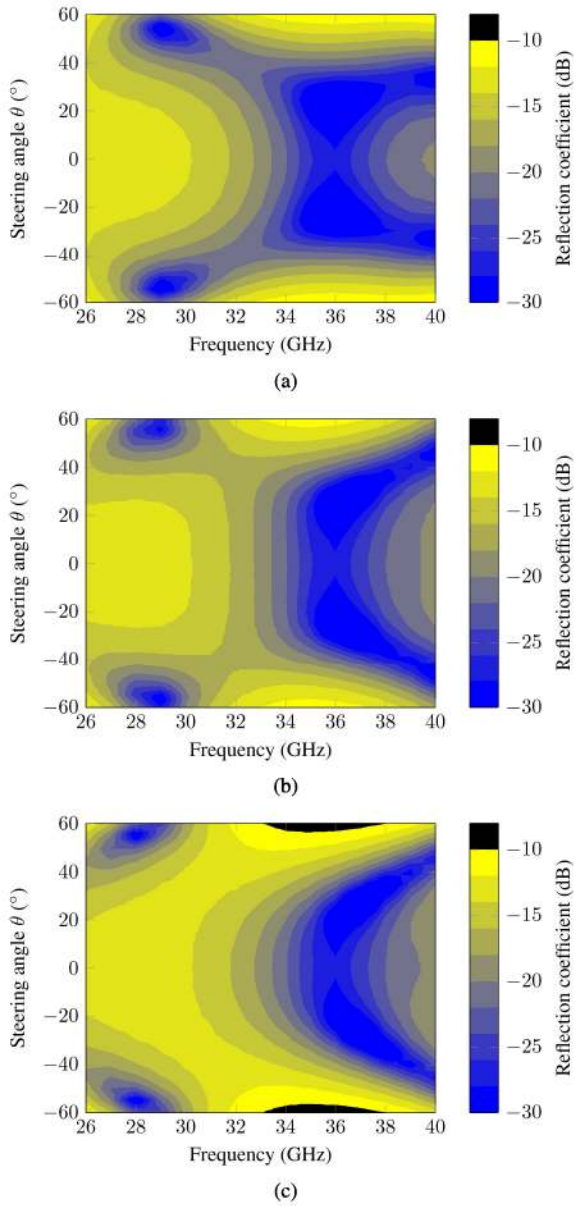

Fig. 3. Active reflection coefficient of the designed antenna element in the unit-cell simulation in planes. (a) $\phi = 0°$, (b) $\phi = 45°$, and (c) $\phi = 90°$ as a function of the steering angle and frequency.

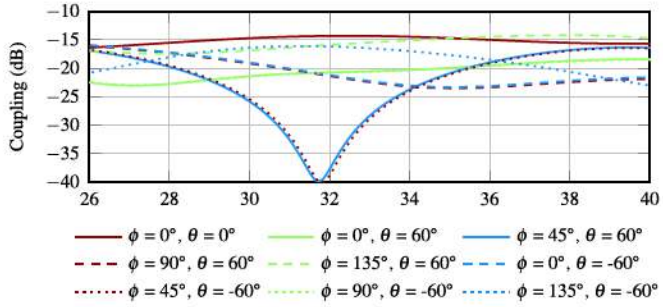

Fig. 4. Coupling between ports for orthogonal polarizations in E-, H-, and D-planes at $\theta = 0°$ and $\theta = 60°$.

The highest coupling is approx. -14 dB in D-plane ($\phi = 135°$) at steering angle $\theta = 60°$.

The total efficiency of the antenna array is generally >90% when the reflection coefficient and the coupling between the ports for different polarizations are taken into account. Also, low conductor losses in the metal structure are assumed. The efficiency falls short of 90% in small number of steering angles close to $\theta = \pm 60°$ when the reflection coefficient is > -10 dB or close to that, while the coupling decreases the efficiency by a few percentages.

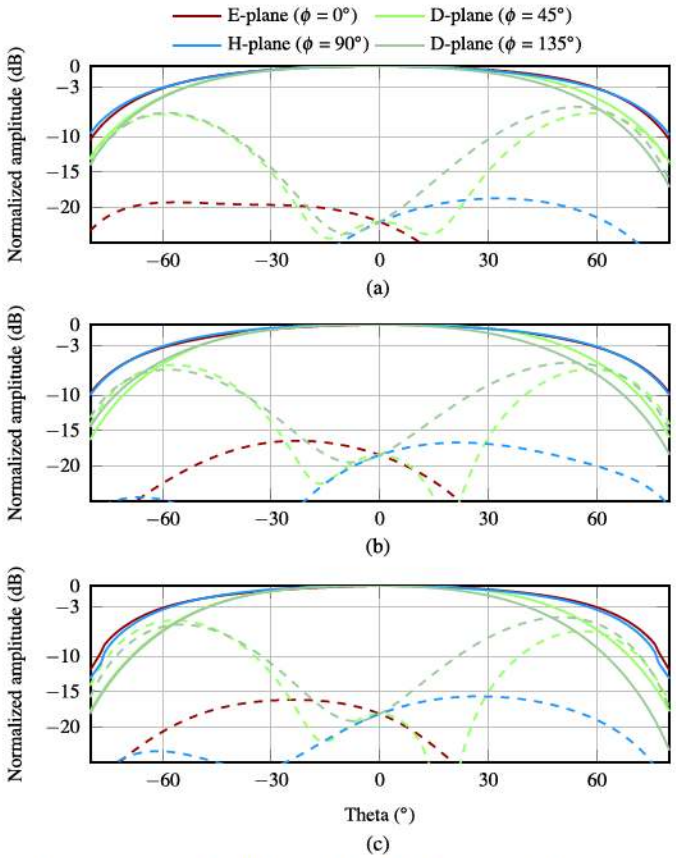

Fig. 5. Normalized co- (solid line) and cross-polarized (dashed line) radiation patterns in the unit-cell simulation in the E-, D-, and H-planes at (a) 26, (b) 33, and (c) 40 GHz.

The co- and cross-polarized components of the element patterns simulated under the infinite-array condition at 26, 33, and 40 GHz are shown in Fig. 5. The simulated co-pol patterns are smooth and symmetric in the E- and H-planes throughout the frequency range. In these planes, the half-power beamwidth is also very large—approximately 120°, which is close to the theoretical beamwidth of an ideal antenna element in an infinite array. At 26 GHz, the cross-pol is primarily below -20 dB, and it is below -15 dB up to 40 GHz in the E- and H-planes. In the D-plane ($\phi = 45°$), the co- and cross-polarized patterns are symmetric, but in the other D-plane ($\phi = 135°$) the patterns are slightly asymmetric due to the asymmetry in the meandered feed line structure. In the D-planes, the cross-pol pattern intersects the co-pol at scan angles $\theta = \pm 73°$, $\pm 63°$, and $\pm 55°$ at 26, 33, and 40 GHz, respectively. On D-plane $\phi = 135°$, when θ is positive, the intersection occurs earlier due to the asymmetry at angles $\theta = 61°$, 55°, and 49°. In the broadside direction, the cross-pol is -22 dB at 26 GHz, whereas at 40 GHz it increases to -18 dB.

The total realized embedded element gain can be calculated from the co-pol and cross-pol components or directly from the

active reflection coefficient using

$$g_{\mathrm{ro}}(\theta,\phi) = \frac{4\pi A}{\lambda^2}\cos(\theta)(1-|R(\theta,\phi)|^2) \tag{4}$$

where A is the area occupied by the radiating element and $R(\theta,\phi)$ is the active reflection coefficient [22]. Calculating the active element pattern from the active reflection coefficient yields a pattern that is very close to the theoretical $\cos(\theta)$-distribution inside the steering range since the reflection coefficient is low (<-10 dB). In finite arrays, the uniformity of co- and cross-pol patterns will suffer slightly, depending on the size of the array due to edge effects. The edge effects will slightly decrease the element beamwidth and introduce variations in the pattern as a function of the steering angle, depending also on the location of the element in the array.

For the prototyping, finite array simulations are done for the antenna elements in four different locations in the dual-polarized 8 × 8 array. The elements are located on two different edges, in the corner and in the middle of the array. The results of the finite array simulation are presented and compared later together with the measurement results.

III. Manufacturing and Measurement Setup

A dual-polarized 8 × 8 antenna array prototype was manufactured to prove that such small elements can be machined without major complications and to study how well the measured performance of the elements in different parts of the array agree with the simulated performance. Four elements in total are examined: one in the middle of the array, one in the corner, and two in the middle of the edges. This helps to understand how the edge of the array affects the pattern of the Vivaldi antenna element.

The 8 × 8 antenna array was manufactured from copper using conventional milling and electric discharge machining (EDM) wire cutting. The bulk material and the coaxial feed pins were first machined using conventional milling and the slot lines and the cavities of the Vivaldi elements that extend through the structure were then cut with EDM wire cutting. The manufactured antenna array is shown in Fig. 6(a), where the orientation of the polarizations and the element numbering is shown. The feeding pins on the bottom of the array are shown in Fig. 6(b). The shape of the single element is seen in Fig. 6(c), and the rectangular grid of elements is visible in Fig. 6(d). The ground plane is 2.3 mm thick and extends approximately 15 mm beyond the edges of the antenna elements and includes holes for mounting and aligning the feed PCB that is situated under the ground plane. Holes for mounting the antenna structure on the measurement holder are also situated on the edges of the ground plane. In this demonstration, the coaxial feeding pins that are used to feed the Vivaldi antennas through the ground plane extend 0.7 mm further.

In this demonstration, where the objective is to measure the shape of the element pattern, to compare the measured and simulated realized gains, and to compare the simulated and measured reflection coefficients of the selected elements, a simple through-hole feeding structure is sufficient. The vertically polarized elements in positions (5,4), (6,1), (1,1), and (1,4) are measured. The corresponding feeding lines 1, 2, 3, and 4 are are shown in Fig. 7. In this setup, the feeding pins are soldered to the pads on the PCB, while the PCB ground plane between the antenna and the substrate is not soldered and relies on capacitive coupling. In actual use case, where all the antenna elements are fed, a surface-mounted antenna is preferred as the through-hole design takes up all the layers in the PCB under the antenna.

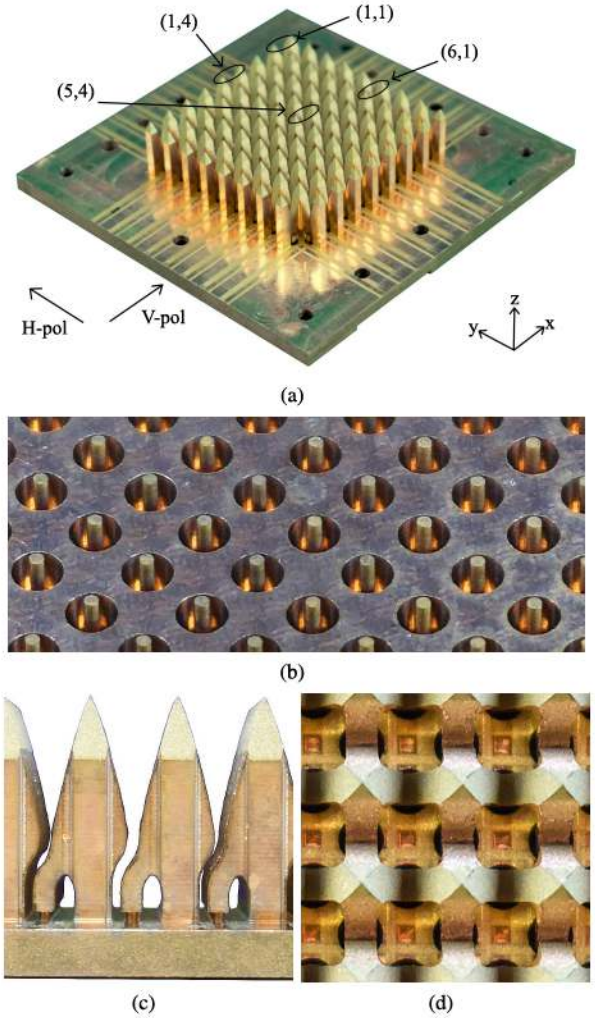

Fig. 6. Manufactured prototype antenna array. (a) General image of the structure. (b) Coaxial feeding pins. (c) Shape of a single element. (d) Rectangular grid arrangement of the elements as seen from the top.

Rogers RO4350B (t = 0.101 mm, $\epsilon_r = 3.48$) is used as the substrate due to its wide availability and low-loss tangent. A transition from a microstrip line to a coaxial line similar to the antenna structure was used to evaluate the effect of the PCB thickness on the matching. A thinner substrate was seen to result in better matching in the through-hole transition. Since the loss tangent of the material is specified up to 10 GHz, 40 mm and 60 mm test microstrip structures were manufactured to determine the losses in the microstrip on the used substrate in order to accurately compare the measured and simulated gains. The losses in the microstrip depend on both the loss tangent of the substrate and the surface roughness of the copper. The loss per centimeter was first measured from the

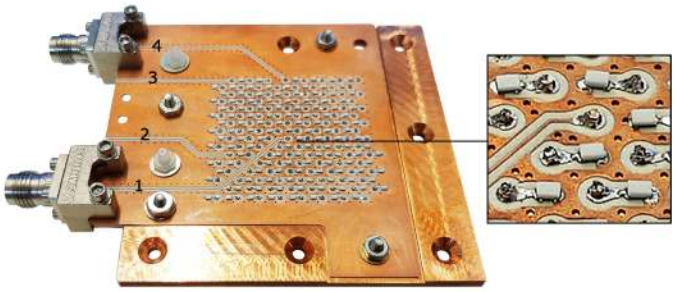

Fig. 7. Assembled prototype. The feeding PCB including microstrips and termination resistors is placed behind the antenna array prototype. The lower end-launch connector is connected to port 1 and the top connector to port 4. Ports 2 and 3 are between the connectors.

manufactured 40 mm and 60 mm long 50 Ω microstrip lines after which the structures were simulated with the nominal loss tangent of 0.00037 and varying surface roughnesses. The measurement and simulation results agree when the surface roughness is 0.8 μm. These values are used in the following simulations.

To feed the selected four elements in different parts of the array, microstrip lines are used as the signal path from the edge of the PCB to the antenna element. In order to measure the radiation pattern of a single element, the other elements are terminated to a matched load to approximate the impedance environment of a fully fed antenna array. 50 Ω Vishay CH-series 0402 thin-film flip-chip resistors are used as the termination loads since they are rated up to 50 GHz and provide a decent termination matching for the passive elements. The assembled array is shown in Fig. 7 from the bottom with all the resistors and feeding pins soldered. 2.4 mm end-launch connectors are used as the interface between coaxial cables and the microstrip lines on the PCB.

IV. Comparison of Simulated and Measured Finite Array–Results and Discussion

In this section, the finite-array simulations and measurements are compared. First, the reflection coefficients from each feed port feeding the single elements in the measurement prototype are measured and compared to the simulated ones for the similar simulation model of an 8 × 8 array with the microstrip line feeds and transitions to the corresponding coaxial pins. The measured results are time gated to exclude the reflections from the end-launch connector in order to compare them more accurately to the simulations where the microstrips are fed with wave ports. Finally, the co- and cross-pol patterns for the middle and corner elements are shown. The radiation patterns for the two edge elements resemble a combination of the middle- and the corner-element patterns. Thus, they are not shown here.

The simulated and time-gated measured reflection coefficients for these four elements are shown in Fig. 8. The shapes of the simulated and measured curves are seen to be close to each other. The measured reflection coefficient of a single element when the other elements are passive and terminated does not directly result in the active reflection coefficient but should also be low around the center of the band. The simulated and measured reflection coefficients are better

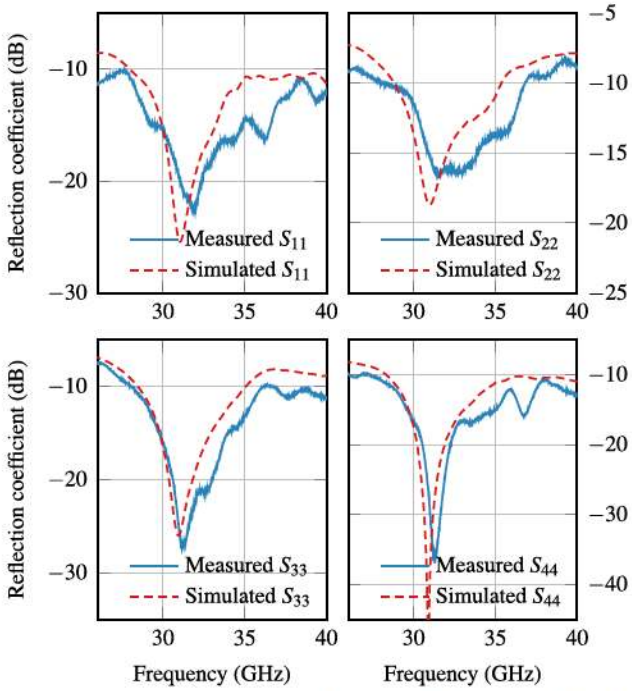

Fig. 8. Simulated and measured reflection coefficient from the end of the microstrip line for the selected element when the other elements are terminated.

than −10 dB at least from 28 to 35 GHz. The simulation model is fully equivalent to the measured prototype, and thus the simulation results for the active reflection coefficient shown in Fig. 3 are considered realistic. We realized that the ripple in the measured reflection coefficient is caused by worse-than-expected matching in the terminated elements. Similar behavior can be replicated in simulations by adding some parasitic inductance and capacitance to the ideal resistor ports. For example, even in an ideal case the total impedance of the resistor diverges from 50 Ω by more than 20% at 40 GHz when mounted [23].

The co- and cross-pol components of the simulated and measured gain pattern of the middle element are shown in Fig. 9 at 26, 33, and 40 GHz. The measured co-pol results of the middle element correspond to the simulation results well at all the presented frequencies with slight additional ripple in the measurements. The measured cross-pol component is generally at a slightly higher level than the simulated one and contains additional ripple. However, the general trend of the measured cross-pol component follows the simulated results. Overall, the simulated and measured results in the 8 × 8 array resemble the predicted results presented previously for the infinite-array case in Fig. 5, where on the diagonal planes the cross-pol level increases with a larger θ angle. The lower level of matching in the termination resistance, which was already noticed in the reflection coefficient measurements, is also responsible for the higher measured cross-pol level compared to simulation results. The level of the cross-pol component increased especially for the middle element when the parasitic inductance in the resistors was increased in the simulation.

As a comparison to the middle element, the co- and cross-pol patterns for the corner element in the same four

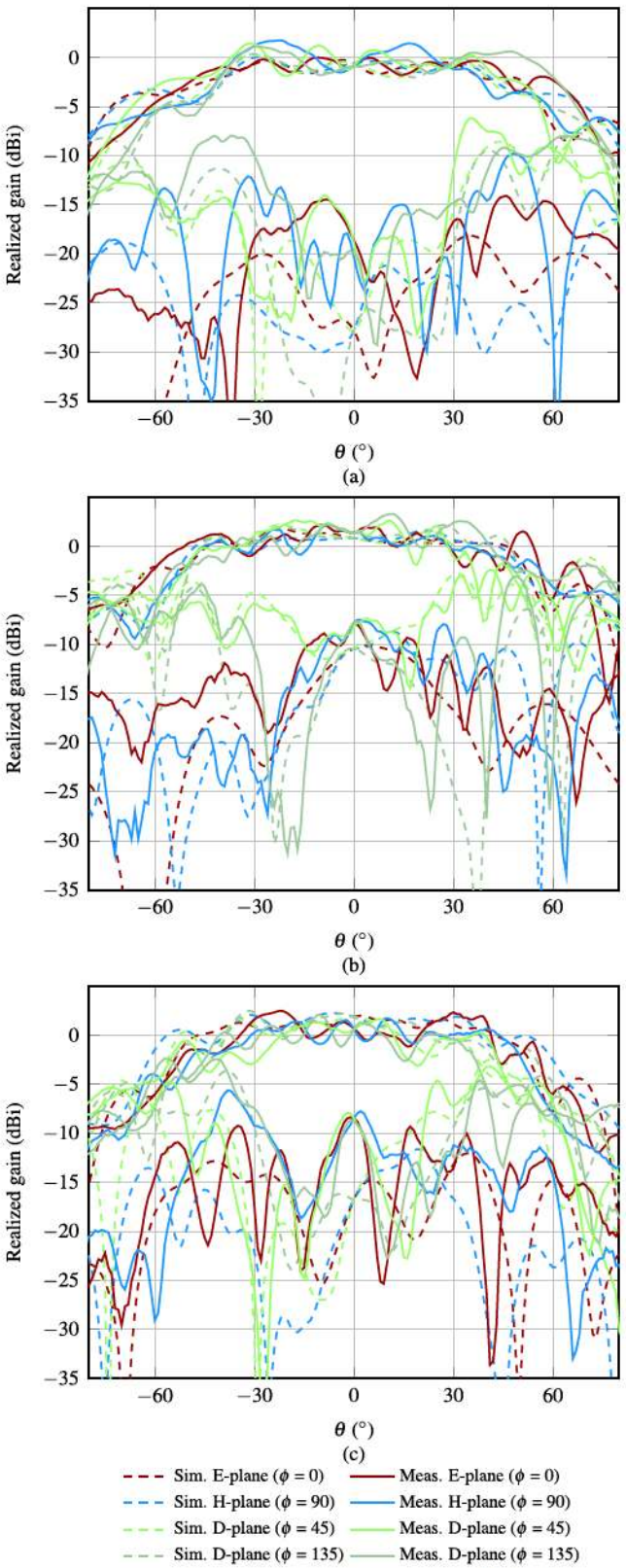

Fig. 9. Simulated and measured co-pol and cross-pol of the (5,4) element in the middle of the array at (a) 26, (b) 33, and (c) 40 GHz in the E-, H-, and D-planes. The same line type is used for the co- and cross-pol patterns in each case.

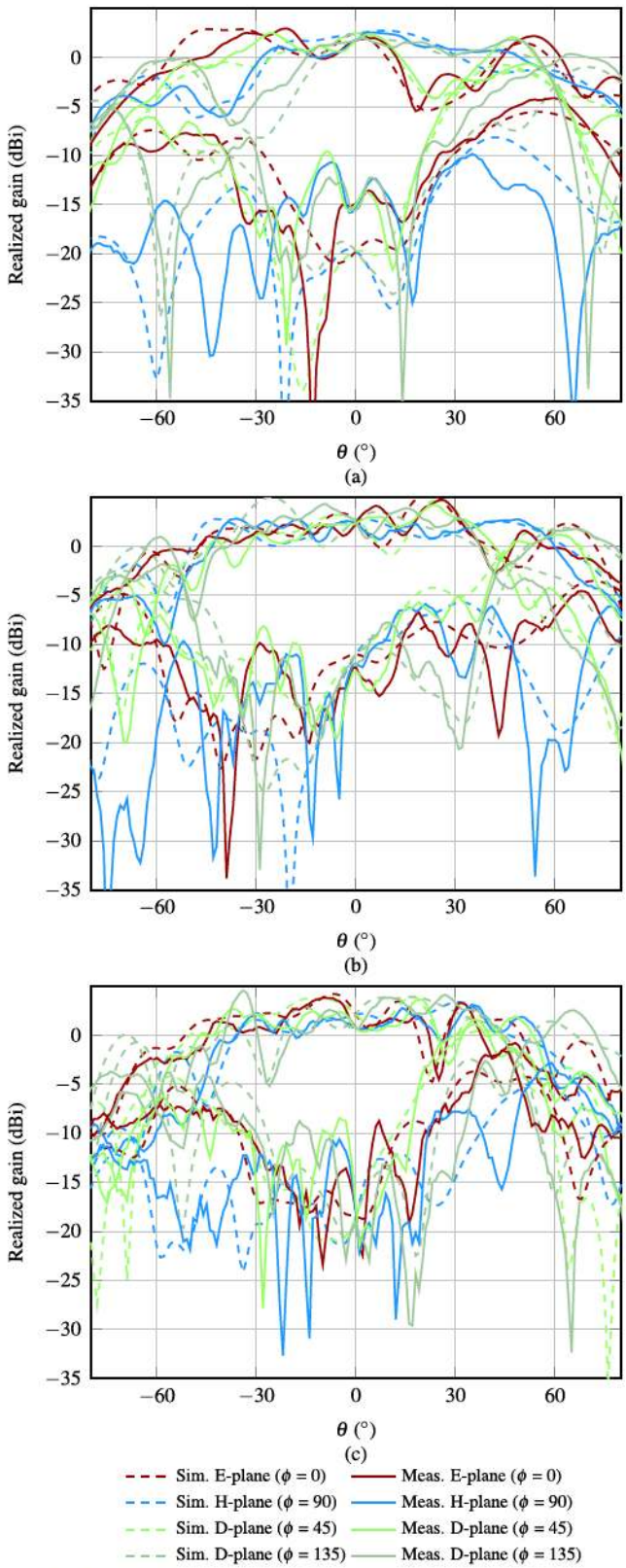

Fig. 10. Simulated and measured co-pol and cross-pol of the (1,1) element in the corner of the array at (a) 26, (b) 33, and (c) 40 GHz in E-, H-, and D-planes. The same line type is used for co- and cross-pol patterns in each case.

planes are shown in Fig. 10. The patterns follow the same trend as the middle element patterns, but the co-pol patterns are less uniform. Additionally, the cross-pol level away from the array increases, whereas toward the array it is affected less. The measured patterns of the corner element are also well in line with the simulations.

Even though the proposed antenna structure is limited in size, the comparison of the results prove that the manufacturing was successful and the antenna structure corresponds well with the simulated model. Since connectors could not be used directly behind each antenna element due to its small size, the PCB with termination resistors and the feed lines to each measured element is used. This solution is not ideal, and the terminations do not work as well as in the simulations and degrade the results. The very close proximity of the neighboring element feeds complicates the use of connectors directly behind each element, and a better solution to characterize the embedded element pattern and the active reflection coefficient should be developed. As the size of the 8×8 array is still relatively small, the measured and simulated embedded element patterns have some ripple but follow the trend of the predicted pattern simulated in the unit cell, i.e., in the infinite-array condition.

V. Conclusion

A dual-polarized fully metallic antenna element for the Ka-band phased array with a scan angle up to 60° without significant polarization degradation is designed and measured. The general shape of the antenna element was optimized with manufacturing and the wide beam-steering range in mind. The fully metallic structure and vertical feed pin through the ground plane allow high efficiency due to the lack of dielectrics in the antenna element. Furthermore, the proposed implementation enables integrating active components close to each antenna element.

The active reflection coefficient in the unit-cell simulation is better than -10 dB through most of the steering and frequency range. There is no scan blindness in the simulated embedded element pattern, and the broadside cross-pol is between -22 and -18 dB over the entire frequency range. As compared to the long Vivaldi elements of [9], this antenna provides an improved co-pol behavior for instance as null-free beam-steering range. This, however, comes at the expense of narrower bandwidth and the further improvement of the cross-pol behavior by reducing the element height would result in a more limited bandwidth.

An 8×8 antenna array prototype was manufactured and the realized gain patterns and reflection coefficients of four elements in different parts of the array were measured. The reflection coefficients from each element and the radiation patterns from the middle and corner elements are presented. The measurement results agree well with those of the finite-array simulations. Both in the finite-array simulations and in the measurements the reflection coefficients from the selected four elements in the passive array are below -10 dB between 29 and 35 GHz.

This article concentrated on studying whether the proposed antenna elements can be manufactured, fed, and measured successfully despite the small size of each antenna element and the close proximity of each feed point. Examination of the single elements in the setup where the rest of the elements are terminated can be used to conclude that the element and antenna array work well when electrically steered. According to these preliminary results, this concept seems very promising for realizing a PCB-mountable high-performance antenna element supporting wideband operation, two polarizations, and passive cooling. Such antennas are needed, for example, in 5G and sensing applications in the Ka-band, where small packaging and wide bandwidth are essential.

The characteristics of the 8×8 array with a complete feeding network to control each element separately will be studied in the future to further investigate the operation of the antenna elements and the surface mounting of the antenna array.

Acknowledgment

The authors would like to thank E. Kahra for helping with the mechanical realization of the prototype and M. Vaaja for assisting with the antenna measurements. They would also like to thank the Project Steering Group at Saab, and especially H. Holter, for discussions and feedback during the project.

References

[1] J. G. Andrews *et al.*, "What will 5G be?" *IEEE J. Sel. Areas Commun.*, vol. 32, no. 6, pp. 1065–1082, Jun. 2014.

[2] T. S. Rappaport *et al.*, "Millimeter wave mobile communications for 5G cellular: It will work!" *IEEE Access*, vol. 1, pp. 335–349, May 2013.

[3] D. Soldani, P. Airas, T. Hoglund, H. Rasanen, and D. Debrecht, "5G to the home," in *Proc. IEEE 85th Veh. Technol. Conf. (VTC Spring)*, Jun. 2017, pp. 1–5.

[4] R. S. Thomä *et al.*, "Cooperative passive coherent location: A promising 5G service to support road safety," 2018, *arXiv:1802.04041*. [Online]. Available: https://arxiv.org/abs/1802.04041

[5] T. Lambard, O. Lafond, M. Himdi, H. Jeuland, S. Bolioli, and L. Le Coq, "Ka-band phased array antenna for high-data-rate SATCOM," *IEEE Antennas Wireless Propag. Lett.*, vol. 11, pp. 256–259, 2012.

[6] A. Chen, Y. Zhang, Z. Chen, and C. Yang, "Development of a *Ka*-band wideband circularly polarized 64-element microstrip antenna array with double application of the sequential rotation feeding technique," *IEEE Antennas Wireless Propag. Lett.*, vol. 10, pp. 1270–1273, 2011.

[7] J. Huang and R. J. Pogorzelski, "A Ka-band microstrip reflectarray with elements having variable rotation angles," *IEEE Trans. Antennas Propag.*, vol. 46, no. 5, pp. 650–656, May 1998.

[8] M. V. Lukic and D. S. Filipovic, "Integrated cavity-backed Ka-band phased array antenna," in *Proc. IEEE Antennas Propag. Soc. Int. Symp.*, Jun. 2007, pp. 133–136.

[9] R. W. Kindt and J. T. Logan, "Benchmarking ultrawideband phased antenna arrays: Striving for clearer and more informative reporting practices," *IEEE Antennas Propag. Mag.*, vol. 60, no. 3, pp. 34–47, Jun. 2018.

[10] H. Holter, "Dual-polarized broadband array antenna with BOR-elements, mechanical design and measurements," *IEEE Trans. Antennas Propag.*, vol. 55, no. 2, pp. 305–312, Feb. 2007.

[11] H. Holter, T.-H. Chio, and D. H. Schaubert, "Experimental results of 144-element dual-polarized endfire tapered-slot phased arrays," *IEEE Trans. Antennas Propag.*, vol. 48, no. 11, pp. 1707–1718, Nov. 2000.

[12] R. W. Kindt and W. R. Pickles, "Ultrawideband all-metal flared-notch array radiator," *IEEE Trans. Antennas Propag.*, vol. 58, no. 11, pp. 3568–3575, Nov. 2010.

[13] S. Livingston and J. J. Lee, "A low profile wide band dual-pol array with coincident phase center for next generation radars," in *IET Int. Conf. Radar Syst. (Radar)*, Oct. 2012, pp. 1–5.

[14] D. H. Schaubert, S. Kasturi, A. O. Boryssenko, and W. M. Elsallal, "Vivaldi antenna arrays for wide bandwidth and electronic scanning," in *Proc. 2nd Eur. Conf. Antennas Propag. (EuCAP)*. Edison, NJ, USA: IET, Nov. 2007, pp. 1–6.

[15] R. Kindt, R. Mital, J. Logan, and M. Vouvakis, "Dual-polarized sliced notch array—Ultra-wideband flares with exceptional polarization control," in *Proc. IEEE Int. Symp. Phased Array Syst. Technol. (PAST)*, Oct. 2016, pp. 1–5.

[16] J. J. Lee, S. Livingston, and R. Koenig, "A low-profile wide-band (5:1) dual-pol array," *IEEE Antennas Wireless Propag. Lett.*, vol. 2, pp. 46–49, 2003.

[17] H. Kähkönen, "Phased antenna array for 26–40 GHz band," M.S. thesis, Dept. Radio Sci. Eng., Aalto Univ., Espoo, Finland, 2017.
[18] J. Shin and D. H. Schaubert, "A parameter study of stripline-fed Vivaldi notch-antenna arrays," *IEEE Trans. Antennas Propag.*, vol. 47, no. 5, pp. 879–886, May 1999.
[19] W. Wasylkiwskyj and W. K. Kahn, "Element patterns and active reflection coefficient in uniform phased arrays," *IEEE Trans. Antennas Propag.*, vol. AP-22, no. 2, pp. 207–212, Mar. 1974.
[20] D. M. Pozar, "A relation between the active input impedance and the active element pattern of a phased array," *IEEE Trans. Antennas Propag.*, vol. 51, no. 9, pp. 2486–2489, Sep. 2003.
[21] D. M. Pozar, "The active element pattern," *IEEE Trans. Antennas Propag.*, vol. 42, no. 8, pp. 1176–1178, Sep. 1994.
[22] P. Hannan, "The element-gain paradox for a phased-array antenna," *IEEE Trans. Antennas Propag.*, vol. 12, no. 4, pp. 423–433, Jul. 1964.
[23] Vishay. (Feb. 2018). *High Frequency 50 GHz Thin Film Chip Resistor, CH Datasheet*. Accessed: Feb. 8, 2018. [Online]. Available: https://www.vishay.com/docs/53014/ch.pdf

Henri Kähkönen was born in Lohja, Finland, in 1989. He received the B.Sc.(tech.) and the M.Sc.(tech.) degrees in electrical engineering from Aalto University, Espoo, Finland, in 2015 and 2017, respectively. He is currently pursuing the D.Sc.(tech.) degree with Saab AB, Helsinki, Finland, and with the Department of Electronics and Nanoengineering, School of Electrical Engineering, Aalto University.

He has been a Research Assistant with Aalto University since 2016. His current research interests include wideband, beam steerable antenna arrays, and especially at millimeter wave spectrum.

Juha Ala-Laurinaho received the Diploma Engineer (M.Sc.) degree in mathematics and the D.Sc.(tech.) degree in electrical engineering from the Helsinki University of Technology (TKK), Espoo, Finland, in 1995 and 2001, respectively.

He has been with TKK, currently Aalto University, serving with the Radio Laboratory from 1995 to 2007, the Department of Radio Science and Engineering from 2008 to 2016, and currently with the Department of Electronics and Nanoengineering. In 1995, he was a Research Assistant. Since 1996, he has been a Research Associate. He is currently a Staff Scientist. He has been a Researcher and a Project Manager in many millimeter wave technology related projects. His current research interests include antennas and antenna measurement techniques for millimeter and submillimeter waves, and the millimeter wave imaging.

Ville Viikari (S'06–A'09–M'09–SM'10) was born in Espoo, Finland, in 1979. He received the M.Sc.(tech.) degree and the D.Sc.(tech.) degree (Hons.) in electrical engineering from the Helsinki University of Technology (TKK), Espoo, in 2004 and 2007, respectively.

From 2001 to 2007, he was with the Radio Laboratory, TKK, where he studied antenna measurement techniques at submillimeter wavelengths and antenna pattern correction techniques. From 2007 to 2012, he was a Research Scientist and a Senior Scientist with the VTT Technical Research Centre, Espoo, where his research included wireless sensors, RFID, radar applications, MEMS, and microwave sensors. He is currently an Associate Professor and the Deputy Head of the Department with the School of Electrical Engineering, Aalto University, Espoo. His current research interests include antennas for mobile networks, RF-powered devices, and antenna measurement techniques.

Dr. Viikari was a recipient of the Young Researcher Award in 2014 by the Finnish Foundation for Technology Promotion, the IEEE Sensors Council 2010 Early Career Gold Award, the 2008 Young Scientist Award of the URSI XXXI Finnish Convention on Radio Science, Espoo, and the Best Student Paper Award of the annual symposium of the Antenna Measurement Techniques Association, Newport, RI, USA, in October 30, 2005 and November 4, 2005. He has served as the Chair of the Technical Program Committee at the ESA Workshop on Millimeter-Wave Technology and Applications and the Global Symposium on Millimeter Waves (GSMM) twice, in 2011 and 2016, Espoo.